CMI

www.nature.com/cmi

ARTICLE

Check for updates

LNCGM1082-mediated NLRC4 activation drives resistance to bacterial infection

Yunhuan Gao[1,2], Yazheng Yang[1], Jianmei Wei[1], Jianmei Yue[1], Ya Wang[1], Qianjing Zhang[1], Mengli Jin[1], Rong Wang[1], Xiaorong Yang[1], Junqi Zhang[3], Xinqi Liu[3], Lin Liu[4], Yuan Zhang[1] and Rongcun Yang[1,2]✉

The activation of NLRC4 is a major host response against intracellular bacteria infection. However, NLRC4 activation after a host senses diverse stimuli is difficult to understand. Here, we found that the lncRNA *LNCGM1082* plays a critical role in the activation of NLRC4. *LNCGM1082* in macrophages affects the maturation of interleukin (IL)-1β and pyroptotic cell death only after exposure to an NLRC4 ligand. Similar to *NLRC4*−/− mice, *LNCGM1082*−/− mice were highly sensitive to *Salmonella* Typhimurium (*S.* T) infection. *LNCGM1082* deficiency in mouse or human macrophages inhibited IL-1β maturation and pyroptosis. Mechanistically, *LNCGM1082* induced the binding of PKCδ with NLRC4 in both mice and humans. In contrast, NLRC4 did not bind PKCδ in *LNCGM1082*−/− macrophages. The activity of the lncRNA *LNCGM1082* induced by *S.* T may be mediated through TLR5 in the macrophages of both mice and humans. In summary, our data indicate that TLR5-mediated *LNCGM1082* activity can promote the binding of PKCδ with NLRC4 to activate NLRC4 and induce resistance to bacterial infection.

Keywords: Macrophages; Inflammasome; lncRNA; Cell pyroptosis; NLRC4; PKCδ

Cellular & Molecular Immunology (2023) 20:475–488; https://doi.org/10.1038/s41423-023-00995-1

INTRODUCTION

NLR family CARD domain-containing 4 (NLRC4) inflammasomes can protect mucosal barriers such as those in the lung, stomach and intestine from invasive bacterial pathogens such as *Salmonella* Typhimurium *(S. T)* [1]. They are formed from multiple cell types, including monocytes, macrophages and nonhematopoietic cells, such as intestinal epithelial cells [1]. The NLRC4 inflammasome is a cytosolic sensor of bacteria that activates caspase-1 and initiates potent immune responses. Activation of NLRC4 inflammasomes includes triggers (e.g., cytosolic flagellin), sensors (NLR apoptosis inhibitory proteins (e.g., NAIPs)), nucleators (e.g., NLRC4), adaptors (e.g., apoptosis-associated speck-like protein (ASC)) and effectors (caspase-1) [2]. Activated caspase-1 together with caspase-11 cleaves and the cytokines IL-1β and IL-18 as well as the pore-forming protein gasdermin D (GSDMD) to generate their mature forms [3, 4]. Mature GSDMD causes pyroptotic cell death and the release of mature IL-1β and IL-18, leading to inflammatory responses that control infection. Pathogenic activators of NLRC4 are mainly derived from gram-negative bacteria, namely, *Salmonella, Legionella, Shigella*, and *Pseudomonas* spp. These bacteria possess flagellin and a Type III (T3SS) or Type IV (T4SS) secretion system comprising rod proteins that are recognized by NAIPs and are unique binding partners of NLRC4 [5, 6]. NLRC4 inflammasome activity depends on NLRC4 activation, which not only relies on NAIP sensing of bacterial components in the cytosol [7] but also NLRC4 phosphorylation [8–11] and ubiquitination [12]. NLRC4 is phosphorylated by PKCδ [8, 10, 11] and leucine-rich repeat kinase 2 (LRRK2) [9]. These kinases form a complex with NLRC4 in macrophages, which leads to the phosphorylation of NLRC4 [8, 9]. However, challenges remain in understanding the regulation of NLRC4 activation after diverse stimuli are recognized.

LncRNAs are transcripts of more than 200 nucleotides that are not translated into proteins. They comprise a heterogeneous class of sense or antisense transcripts, intergenic transcripts and enhancer RNAs [13]. LncRNAs carry out diverse functions, including the regulation of protein or RNA molecule production, transcriptional regulation in cis or trans, organization of nuclear domains [14] and allosteric regulation of enzymatic activity [15, 16]. Some transcripts have been annotated as lncRNAs encode small proteins [17]. The overexpression, deficiency and mutation of lncRNA genes have been implicated in numerous human diseases [18]. In this study, we found that *LNCGM1082* plays a critical role in the activation of NLRC4. *LNCGM1082* in macrophages inhibited the maturation of interleukin (IL)-1β and pyroptotic cell death but only after exposure to NLRC4 ligand. We found that *LNCGM1082* induced the binding of PKCδ with NLRC4 in both mice and humans. This lncRNA was induced by *S.* T mediated through TLR5 action in the macrophages in both mice and humans. Hence, the activity of *LNCGM1082* induced by TLR5 mediates the binding of PKCδ with NLRC4 to activate NLRC4 and induce resistance to bacterial infection.

[1]Department of Immunology, Nankai University School of Medicine and Translational Medicine Institute, Affiliated Tianjin Union Medical Center of Nankai University, Nankai University, Tianjin 300071, China. [2]State Key Laboratory of Medicinal Chemical Biology, Nankai University, Tianjin 300071, China. [3]College of Life Science, Nankai University, Tianjin 300121, China. [4]China National Center for Bioinformation & Beijing Institute of Genomics, Chinese Academy of Sciences, Beijing, China. ✉email: ryang@nankai.edu.cn

Received: 19 June 2022 Accepted: 23 February 2023
Published online: 20 March 2023

RESULTS

LNCGM1082 in macrophages promotes IL-1β maturation and pyroptosis

We investigated the effects of lncRNAs on myeloid-derived suppressive cells (MDSCs), and multiple lncRNAs were found to be highly expressed in MDSCs [19] (Fig. 1A). Since macrophages are derived from myeloid cells, we evaluated the expression of these lncRNAs in macrophages. The data showed that certain lncRNAs highly expressed in MDSCs were also highly expressed in macrophages (Supplementary Fig. 1). Since macrophages play critical roles in protecting against invasive bacterial pathogens via the release of IL-1β and induction of pyroptosis [1], we next identified these lncRNAs. Only the *lncRNA GM-1082* (*LNCGM1082*) exerted an effect on IL-1β production and pyroptosis (Supplementary Fig. 1). Therefore, we further investigated the expression and function of *LNCGM1082*. In addition to macrophages, *LNCGM1082* was expressed in dendritic cells but not in $CD4^+$ or $CD8^+$ T cells or $CD19^+$ B cells (Fig. 1B). *LNCGM1082* expression in macrophages obtained from the peritoneal cavity of thioglycollate-treated mice was confirmed using fluorescence in situ hybridization (FISH) and Northern blotting (Fig. 1C, D). Except where specifically indicated, macrophages isolated from the peritoneal cavity of thioglycollate-treated mice were used in the study. Mouse *LNCGM1082* is located on Chromosome 7, whereas human *LNCGM1082* is located on Chromosome 19 (Supplementary Fig. 2A). *LNCGM1082* predominantly localizes to the cytoplasm (Fig. 1C).

We next further investigated the function(s) of *LNCGM1082* in macrophages. Indeed, when macrophages were primed with lipopolysaccharide (LPS) and subsequently treated with flagellin (LPS with flagellin) [20], *LNCGM1082* promoted a marked increase in mature IL-1β production (Fig. 1E, F). LPS, LPS with DOTAP, LPS with nigericin or LPS with poly (dA and dT) did not cause significant changes in mature IL-1β level in these macrophages (Fig. 1E, F). Since mature IL-1β production often coincides with pyroptosis [3, 4], which is lytic cell death induced by pathogen infection or endogenous challenge [21], we also investigated the pyroptosis rate in *LNCGM1082* shRNA- or exogenous *LNCGM1082*-transfected macrophages after exposure to LPS with flagellin. The data showed that silencing *LNCGM1082* markedly reduced the pyroptosis rate, whereas exogenous *LNCGM1082* promoted pyroptosis in macrophages (Fig. 1G, H). LPS, LPS with DOTAP, LPS with nigericin or LPS with poly (dA and dT) also induced pyroptosis, but no difference was found in *LNCGM1082 shRNA*- or exogenous *LNCGM1082*-transfected macrophages (Fig. 1G, H). Multiple pathways induce IL-1β maturation and pyroptosis, including those primed by NLRC4, caspase-11 and NLRP3. LPS with flagellin is an activator of NLRC4 [2]; LPS with DOTAP is an activator of caspase-11 [22]; LPS with nigericin activates NLRP3 [23]; and LPS with poly (dA and dT) is recognized by multiple PRRs, including cytosolic DNA sensors (CDSs) such as cGAS, AIM2, DAI, DDX41, IFI16, and LRRFIP1 [24]. *LNCGM1082*-transfected macrophages exhibited differences in mature IL-1β production and pyroptosis only in response to LPS with flagellin (NLRC4 ligand) but not LPS with nigericin (NLRP3 ligand), LPS with DOTAP or LPS with poly (dA and dT) (CDS ligands), suggesting that *LNCGM1082*-mediated IL-1β and pyroptosis may be mediated through the action of NLRC4.

LNCGM1082 exerts regulatory effects similar to those of NLRC4 on the maturation of IL-1β and pyroptosis of macrophages

To further determine the function(s) of *LNCGM1082* in macrophages, we generated *LNCGM1082*-deficient mice. Macrophages were isolated from wild-type (wt) and *LNCGM1082*−/− mice. The deletion of *LNCGM1082* did not affect the expression of two adjacent genes, arhgap 33 or prodh2, in mice (Supplementary Fig. 2B, C). After exposure to LPS with flagellin (an NLRC4 ligand), LPS with DOTAP (a caspase-11 ligand), LPS with nigericin (an NLRP3 ligand) or LPS with poly (dA and dT) (CDS ligands), only LPS with flagellin treatment led to decreased levels of mature IL-1β or IL-18 but not to the transcript levels of IL-1β in *LNCGM1082*−/− macrophages (Fig. 2A), further suggesting that *LNCGM1082* exerts an effect on the NLRC4-mediated pathway. Therefore, we next compared *LNCGM1082*−/− macrophages with those from *NLRC4*−/− mice. The data showed similar effects in *LNCGM1082*−/− and *NLRC4*−/− macrophages exposed to LPS with flagellin or *S.* T (Fig. 2B, C), which differed from the effects observed i *caspase-1/11*−/− and *NLRP3*−/− macrophages. *LNCGM1082*−/− and *NLRC4*−/− macrophages showed reduced IL-1β and IL-18 maturation rates after exposure to LPS with flagellin or *S.* T but not after treatment by LPS with nigericin (Fig. 2B, C). We also investigated the effects of *LNCGM1082* on the pyroptosis rate of macrophages. Similar resistance to flagellin-mediated pyroptosis between *LNCGM1082*−/− and *NLRC4*−/− macrophages was also observed after exposure to LPS with flagellin but not to LPS with nigericin (Fig. 2D–F). In addition, the macrophages from *caspase-1/11*−/− and *NLRP3*−/− mice exhibited different pyroptosis rates from those of *LNCGM1082*−/− macrophages after exposure to LPS with flagellin, LPS with nigericin or *S.* T (Fig. 2D–F). The other effects of *LNCGM1082* on macrophages were investigated through microarray assays. However, very few genes were differentially expressed between wt and *LNCGM1082*−/− macrophages, implying that *LNCGM1082* is involved in very few functions in addition to the inhibition of IL-1β action and pyroptosis(Supplementary Fig. 3). Notably, the peptides encoded by another transcript, *arhgap33os-202*, which was encoded by the same gene as that encodes *LNCGM1082* or by the Open Reading Frame 2 or 8 in *LNCGM1082*, which potentially encodes peptides, did not lead to a significant effect on flagellin-mediated activation of NLRC4 (Supplementary Fig. 4). Taken together, these results suggest that *LNCGM1082* may play roles similar to that of NLRC4 in inhibiting IL-1β maturation and pyroptosis in macrophages.

NLRC4−/− mice and *LNCGM1082*−/− mice are highly sensitive to *Salmonella*. infection

Since *LNCGM1082*−/− mice to express regulatory genes similar to those expressed in *NLRC4*−/− mice to inhibit IL-1β maturation and pyroptosis in macrophages exposed to flagellin, we employed an *S.* T infection model, which we used to identify the role(s) of NLRC4 [25] and further assess the role of *LNCGM1082*. *LNCGM1082*−/−, *NLRC4*−/− and control mice were individually infused with *S.* T (200 CFUs/mouse). Then, we observed the changes in body weight and survival rate. Similar to previous reports [26], *NLRC4*−/− mice presented with markedly reduced body weights and survival rates. *LNCGM1082*−/− mice showed body weight changes and survival rates similar to those of the *NLRC4*−/− mice (Fig. 3A, B). Bacteria can colonize and infect anatomical sites in addition to the gastrointestinal tract in a mammalian host, including the lungs, liver and spleen [27–29]. Similar to *NLRC4*−/− mice [27–29], *LNCGM1082*−/− mice succumbed to infection more quickly and showed an increased bacterial burden in the lung, liver and spleen compared with that in wt mice (Fig. 3C–E). These *LNCGM1082*−/− mice also showed reduced inflammation in lung tissues and a decreased IL-1β level in serum and inflammatory cells (Fig. 3F–H). In addition, we compared *LNCGM1082*−/− mice with *caspase-1/11*−/− or *NLRC3*−/− mice, and the *NLRP3*−/− and *caspase-1/11*−/− mice showed different sensitivities to *S. T* infection compared to that shown by *LNCGM1082*−/− mice (Fig. 3A–H). Since *S.* T infection causes inflammation of not only gut epithelial cells but also gut macrophages [30, 31], we transplanted bone marrow cells into irradiated recipients to identify the involvement of gut macrophages. WR mice carrying reconstituted *LNCGM1082*−/− bone marrow showed an elevated bacterial in the liver, lung and spleen compared with that in wt mice with reconstituted wt bone marrow (Supplementary Fig. 5), indicating that macrophages play

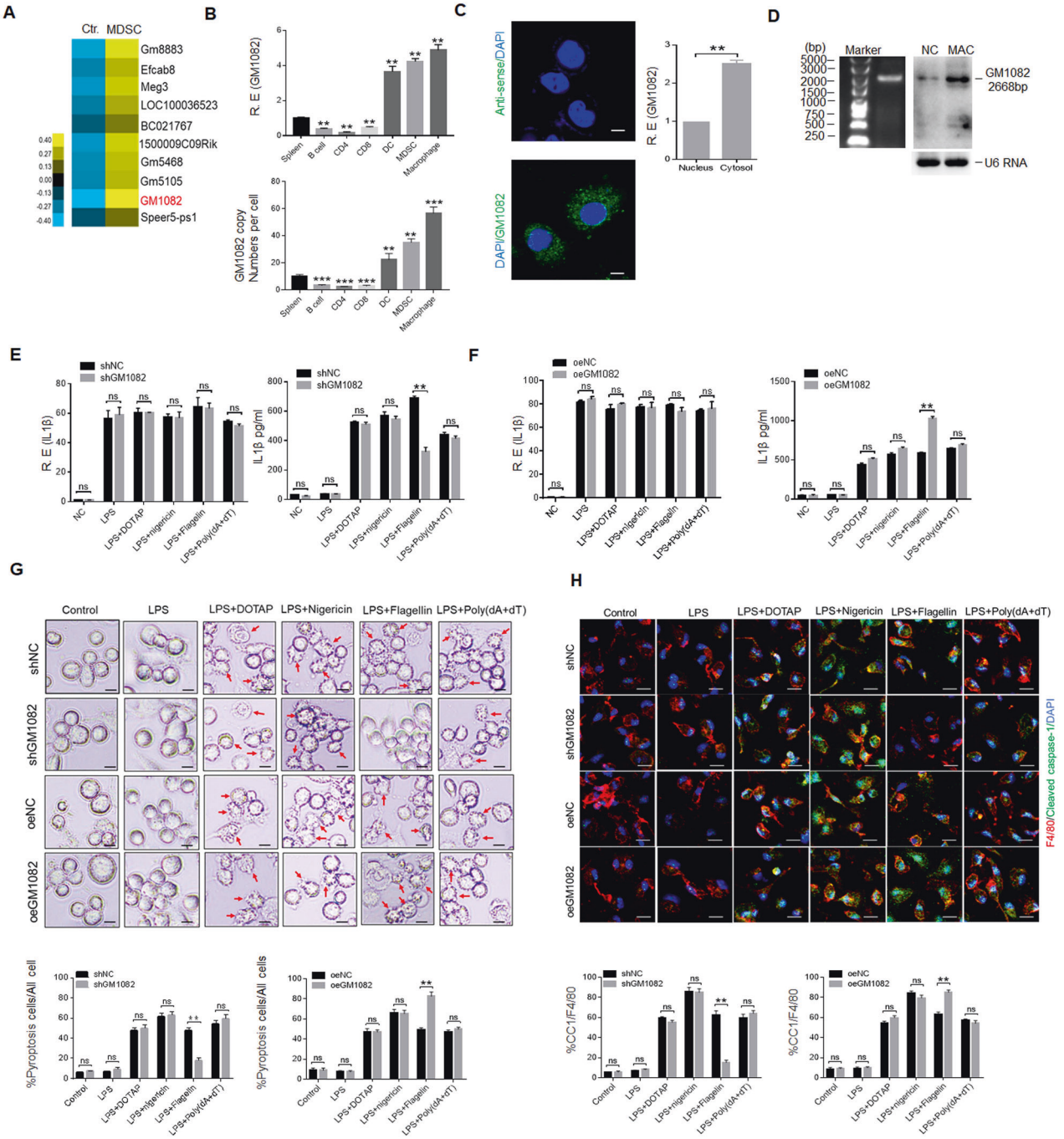

Fig. 1 *LNCGM1082* promotes IL-1β maturation and pyroptosis in macrophages. **A** LncRNA microarray prepared from myeloid derived suppressor cells (MDSCs). MDSCs were generated, and lncRNA expression was evaluated using a lncRNA expression microarray. Ctr., bone marrow cells. **B** qRT–PCR of *LNCGM1082* in the spleen, B cells, CD4 T cells, CD8 T cells, dendritic cells (DC), MDSCs and macrophages from spleen sorted by flow cytometry. R E., relative expression. **C** Fluorescence in situ hybridization of *LNCGM1082* in mouse macrophages and qRT–PCR analysis of *LNCGM1082* in the cytosol and nucleus. Nuclei were stained with DAPI (blue); green, *LNCGM1082*. Scale bar, 2.5 μM. **D** Northern blot showing murine *LNCGM1082* in mouse macrophages. NC, bone marrow cells; MAC, macrophages. **E**, **F** qRT–PCR of IL-1β and ELISA of IL-1β in the supernatants of wt, *LNCGM1082* shRNA (shLNCGM1082)- and exogenous *LNCGM1082* (oeLNCGM1082)-transfected macrophages, which were stimulated by different stimuli. R.E., relative expression. **G** Images of *LNCGM1082* shRNA (shLNCGM1082)- and exogenous *LNCGM1082* (oeLNCGM1082)-transfected macrophages under light microscopy after stimulation with LPS plus DOTAP, LPS plus nigericin, LPS plus flagellin or LPS plus poly(dA+dT). Scale bar, 5 μM. The arrows indicate pyroptotic cells. **H** Confocal microscopy image showing immunofluorescence staining of caspase-1 fragments in *LNCGM1082* shRNA (shLNCGM1082)- and exogenous *LNCGM1082* (oeLNCGM1082)-transfected macrophages after stimulation with LPS plus DOTAP, LPS plus nigericin, LPS plus flagellin or LPS plus poly(dA+dT). Macrophages were isolated from the peritoneal cavity of thioglycollate-treated mice. Scale bar, 5 μM. Student's *t* test were performed with the data shown in (**B**), (**C**) and (**E**)–(**H**); the mean ± SD; n.s., not significant; **, $p < 0.01$; ***, $p < 0.001$

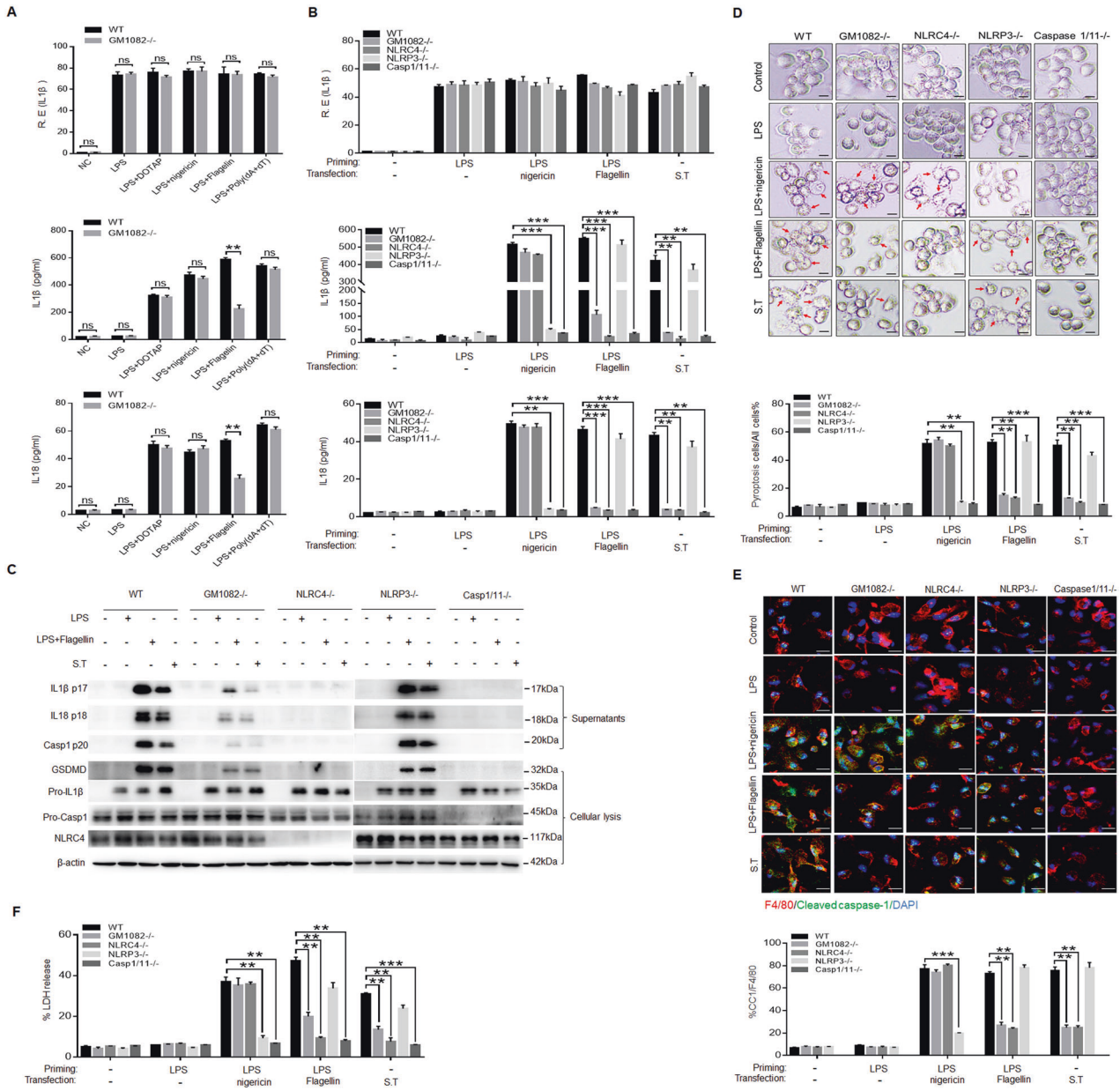

Fig. 2 *LNCGM1082−/−* macrophages are similar to *NLRC4−/−* macrophages in terms of IL-1β maturation and pyroptosis. **A** qRT–PCR assay of IL-1β and ELISAs of IL-1β and IL18 levels in the supernatants of wt and *LNCGM1082−/−* macrophages after stimulation by different stimuli. R.E., relative expression. **B** qRT–PCR assay of IL-1β and ELISAs of IL-1β and IL18 levels in the supernatants of wt, *LNCGM1082−/−*, *NLRC4−/−*, *NLRP3−/−* and *caspase-1/11−/−* macrophages stimulated by LPS plus nigericin or LPS plus flagellin treatment or infected by *S.* T. R.E., relative expression. **C** Western blots showing the proteins in macrophages and their supernatants after stimulation with LPS plus flagellin treatment or *S.* T infection. **D** Images showing the macrophages under light microscopy after stimulation with LPS plus nigericin or LPS plus flagellin treatment or *S.* T infection. The arrows indicate pyroptotic cells. Scale bar, 5 μM. **E** Immunostained caspase-1 fragments in macrophages after stimulation with LPS plus nigericin or LPS plus flagellin treatment or *S.* T infection. **F** LDH in the supernatants of macrophages stimulated by LPS plus nigericin or LPS plus flagellin treatment or *S.* T infection. Student's *t* test was performed with the data in **A**, **B** and **D**, **F**; the mean ± SD; n.s., not significant; **, $p < 0.01$; ***, $p < 0.001$

a main role in the response to *S.* T infection. We also performed LPS toxicity experiments, and no differences were found between *LNCGM1082−/−* and wt mice (Supplementary Fig. 6), implying that no relationship between *LNCGM1082* and caspase-11 [32]. In addition, enteropathogenic *E. coli* can activate NLRC4 [26]. Equal amounts of GFP-labeled *Escherichia coli*, which were isolated from DSS-mediated colitis and previously demonstrated to promote inflammation [33], were infused into both *LNCGM1082−/−* and *NLRC4−/−* mice, and these mice showed similar increases in bacteria levels compared to the level in wt mice, as measured in feces 2 days after infusion (Fig. 3I). Taken together, these results indicate that similar to *NLRC4−/−* mice, *LNCGM1082−/−* mice are highly sensitive to *S.* T and *E. coli* infection.

Binding of *LNCGM1082* with NLRC4 and PKCδ induces NLRC4 phosphorylation

Since lncRNAs may function directly by binding with proteins [15], we sought to determine whether *LNCGM1082* binds with NLRC4 to regulate NLRC4 function. We first examined NLRC4 phosphorylation in macrophages exposed to *S. T* or flagellin. *LNCGM1082−/−* macrophages showed abolished phosphorylation of NLRC4 (Fig. 4A). NLRC4 is phosphorylated through PKCδ [8, 10, 11] or

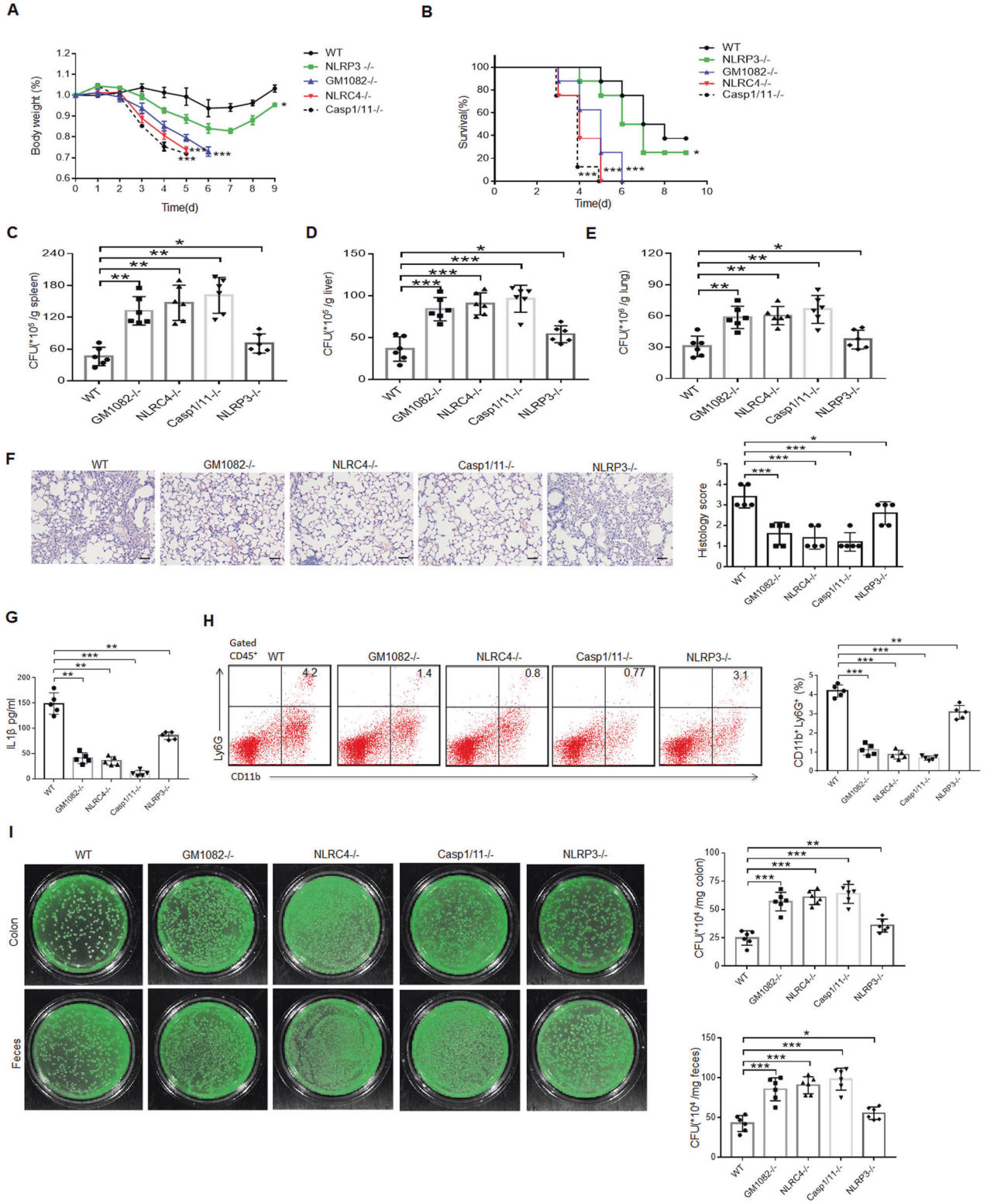

Fig. 3 *NLRC4−/−* mice and *LNCGM1082−/−* mice were similarly sensitive to *S.* T infection. **A** Body weight of wt, *LNCGM1082−/−*, *NLRC4−/−*, *NLRP3−/−* and *Caspase-1/11−/−* mice after *S.* T infection. **B** Survival rate of wt, *LNCGM1082−/−*, *NLRC4−/−*, *NLRP3−/−* and *caspase-1/11−/−* mice after *S.* T infection. Bacterial CFUs in the spleen (**C**), liver (**D**) and lung (**E**) of wt, *LNCGM1082−/−*, *NLRC4−/−*, *NLRP3−/−* and *caspase-1/11−/−* mice after *S. T* infection. **F** H&E stained lung sections from the mice shown in (**A**). Scale bar, 80 μm. **G** ELISA of IL-1β level in the blood collected from mice shown in (**A**). **H** Flow cytometry of neutrophils ($CD11b^+$ $Ly6G^+$) from the intestinal lamina propria of mice shown in (**A**). The percentages of $CD11b^+$ $Ly6G^+$ neutrophils were compared ($n = 5$). **I** Bacterial burden in the colon and feces of wt, *LNCGM1082−/−*, *NLRC4−/−*, *NLRP3−/−* and *caspase-1/11−/−* mice after GFP-labeled *Escherichia coli O160* infection. Analysis of variance test was performed with the data shown in (**A**); Wilcoxon's test was performed with the data shown in (**B**); two-sided Student's *t* test was performed with the data shown in (**C**)–(**I**). *, $p < 0.05$; **, $p < 0.01$; ***, $p < 0.001$

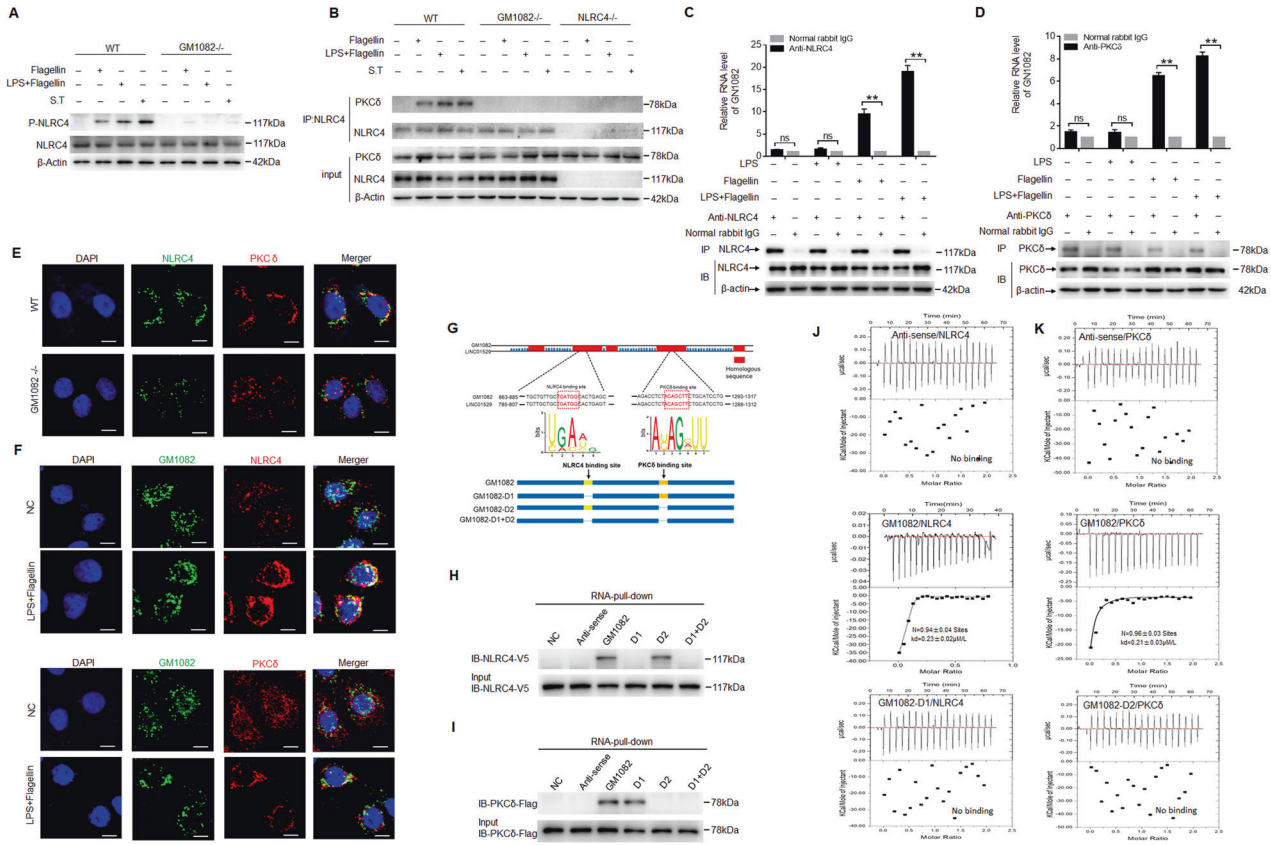

Fig. 4 Binding of LNCGM1082 with NLRC4 and PKCδ induced NLRC4 phosphorylation. **A** Immunoblots showing phosphorylated NLRC4 in macrophages after exposure to *S*. T.or flagellin. **B** Immunoblot showing NLRC4 and PKCδ in macrophages. Immunoprecipitation was performed using anti-NLRC4 antibody, and then, immunoblotting was performed using anti-PKCδ antibody. **C**, **D** RIP with macrophages after exposure to flagellin or *S*. T. Cell lysates were incubated with normal rabbit IgG and anti-NLRC4 and anti-PKCδ antibodies. The immunoprecipitates were analyzed by qRT–PCR to determine the *LNCGM1082* level **E** Immunostaining for NLRC4 and PKCδ in wt and *LNCGM1082*−/− macrophages. Red, PKCδ; green, NLRC4. blue, nuclei. Scale bar, 2.5 μM. **F** Immunostaining and RNA-FISH of NLRC4, PKCδ and *LNCGM1082* in macrophages. Red, NLRC4 or PKCδ; green, *LNCGM1082*; blue, nuclei. Scale bar, 2.5 μM. **G** Construction of LNCGM1082 plasmids (pCDNA3.1) lacking the D1, D2, or D1 + D2 sites. We used the NCBI database to perform sequence comparisons and identify homologous sequences and MEME software (https://meme-suite.org/meme/) to identify the NLRC4 and PKCδ protein binding motifs. NLRC4- and PKCδ-binding sites were named "D1" and "D2", respectively. *LNCGM1082* plasmids lacking D1, D2 or D1 + D2 sites were constructed. **H**, **I** RNA pull-down assay using biotinylated *LNCGM1082* and *LNCGM1082* fragments from V5-tagged NLRC4- or flag-tagged PKCδ-transfected HEK293T cells. NC, no biotinylated *LNCGM1082* or fragments. **J**, **K** ITC analysis of the binding of mouse *LNCGM1082* and mutated *LNCGM1082* (deletion of D1 or D2) to NLRC4 and PKCδ. Two-sided Student's *t* test was performed with the data shown in (**C**) and (**D**). n.s., not (statistically) significant; **, $p < 0.01$

LRRK2 [9], which form a complex with NLRC4 in macrophages. This process mediates IL-1β production and cellular pyroptosis, which were inhibited by silencing related proteins, such as PKCδ (Supplementary Fig. 7), consistent with other studies [8, 10, 11]. Immunoprecipitation (IP) revealed that NLRC4 did not bind with PKCδ in *LNCGM1082*−/− macrophages; similarly NLRC4 did not bind with PKCδ in *NLRC4*−/− macrophages (Fig. 4B). These findings suggest that *LNCGM1082* might bind with NLRC4 and PKCδ. Indeed, RNA immunoprecipitation analyses (RIPs) showed that *LNCGM1082* not only bound NLRC4 but also PKCδ (Fig. 4C, D). These binding events were confirmed through FISH and coimmunostaining of *LNCGM1082* with NLRC4 and PKCδ (Fig. 4E, F). Marked binding of NLRC4 and PKCδ was observed in the macrophages of wt mice, whereas these binding events were not evident in the *LNCGM1082*−/− macrophages exposed to flagellin and LPS (Fig. 4E, F). Furthermore, the binding of *LNCGM1082* with NLRC4 and PKCδ was confirmed (Supplementary Fig. 8A, B).

We next wanted to find the potential motif in *LNCGM1082* that is bound by NLRC4 or PKCδ. We first used the iCLIP truncation track to show the positions of iCLIP cDNA truncations at *LNCGM1082* with the peak heights corresponding to the cDNA counts (Supplementary Fig. 9A). Then, we obtained lncRNAs by RIP using an anti-NLRC4 antibody and digested them with RNA enzymes to establish a cDNA library after amplification. A potential binding motif in *LNCGM1082*, which interacted with NLRC4 according to MEME algorithm analyses, was identified (Supplementary Fig. 9B). We also predicted the binding sites of PKCδ on *LNCGM1082* using RNAInter software (http://www.rna-society.org/raid/home.html) (Supplementary Fig. 9C). The sequence logo of the PKCδ-recognition motif was generated by MEME analysis of lncRNA sequence read clusters (Supplementary Fig. 9D). We named the NLRC4 binding site "D1" and the PKCδ binding site "D2" and constructed mutated *LNCGM1082* plasmids that lacked the D1, D2, or D1 + D2 sites (Fig. 4G). RNA pull-down assays demonstrated that the D1 fragment of *LNCGM1082* could bind with NLRC4, whereas D2 was essential for PKCδ (Fig. 4H, I). The binding of *LNCGM1082* with NLRC4 and PKCδ was confirmed by isothermal titration calorimetry (ITC) analyses (Fig. 4J, K). The ITC data also confirmed that the D1 and D2 fragments were necessary for the binding of *LNCGM1082* with NLRC4 and PKCδ (Fig. 4J, K). To confirm the binding of *LNCGM1082* with NLRC4 and PKCδ in cells, we cloned NLRC4, PCK δ and their fragments with tagged V5 (Supplementary Fig. 10) and then cotransfected the fragments cells with *LNCGM1082* into HEK293T cells. RIP using an anti-V5

antibody with cotransfected HEK293T cells showed the binding of *LNCGM1082* with NLRC4 and PKCδ (Supplementary Fig. 10B, C, E). Furthermore, the LRR region in NLRC4 and the C4 region in PKCδ were found to be critical to the binding of NLRC4 with *LNCGM1082* (Supplementary Fig. 10B, E). In addition, *LNCGM1082* inhibited the oligomerization of apoptosis-associated speck-like protein containing a CARD (ASC) and speck formation (Supplementary Fig. 11). Since LRRK2 induces the activation of NLRC4, we also measured the binding of *LNCGM1082* with LRRK2 [9]. The data did not show an interaction between *LNCGM1082* and LRRK2 (Supplementary Fig. 12A). In addition, caspase-1, caspase-11 and NLRP3 regulate the production of mature IL-1β and pyroptosis, but the data did not show the binding of *LNCGM1082* with caspase-1, caspase-11, or NLRP3 (Supplementary Fig. 12B–D). Taken together, these data indicate that *LNCGM1082* binds with NLRC4 and PKCδ to induce the phosphorylation of NLRC4.

The functions of *LNCGM1082* are similar in mouse and human macrophages

LNCGM1082 is highly conserved between mouse and human, showing 43.85% homology. NLRC4 and PKCδ are also highly conserved between humans and mice, as indicated by an analysis performed with DNAMAN software. We next investigated whether *LNCGM1082* plays a similar role in mouse and human macrophages. We first detected the expression of *LNCGM1082* in human macrophages. The THP-1 human monocyte/macrophage cell line and primary macrophages from colon tissues expressed human *LNCGM1082* (Fig. 5A). THP-1 cells recognized flagellin from *S.* T [34, 35]. To identify the function(s) of *LNCGM1082* in human macrophages, we generated *huLNCGM1082*−/− THP-1 macrophages using the CRISPR CAS9 gene knockout technique and confirmed that *huLNCGM1082* was knocked out (Fig. 5A). The deletion of *LNCGM1082* did not affect the expression of two adjacent

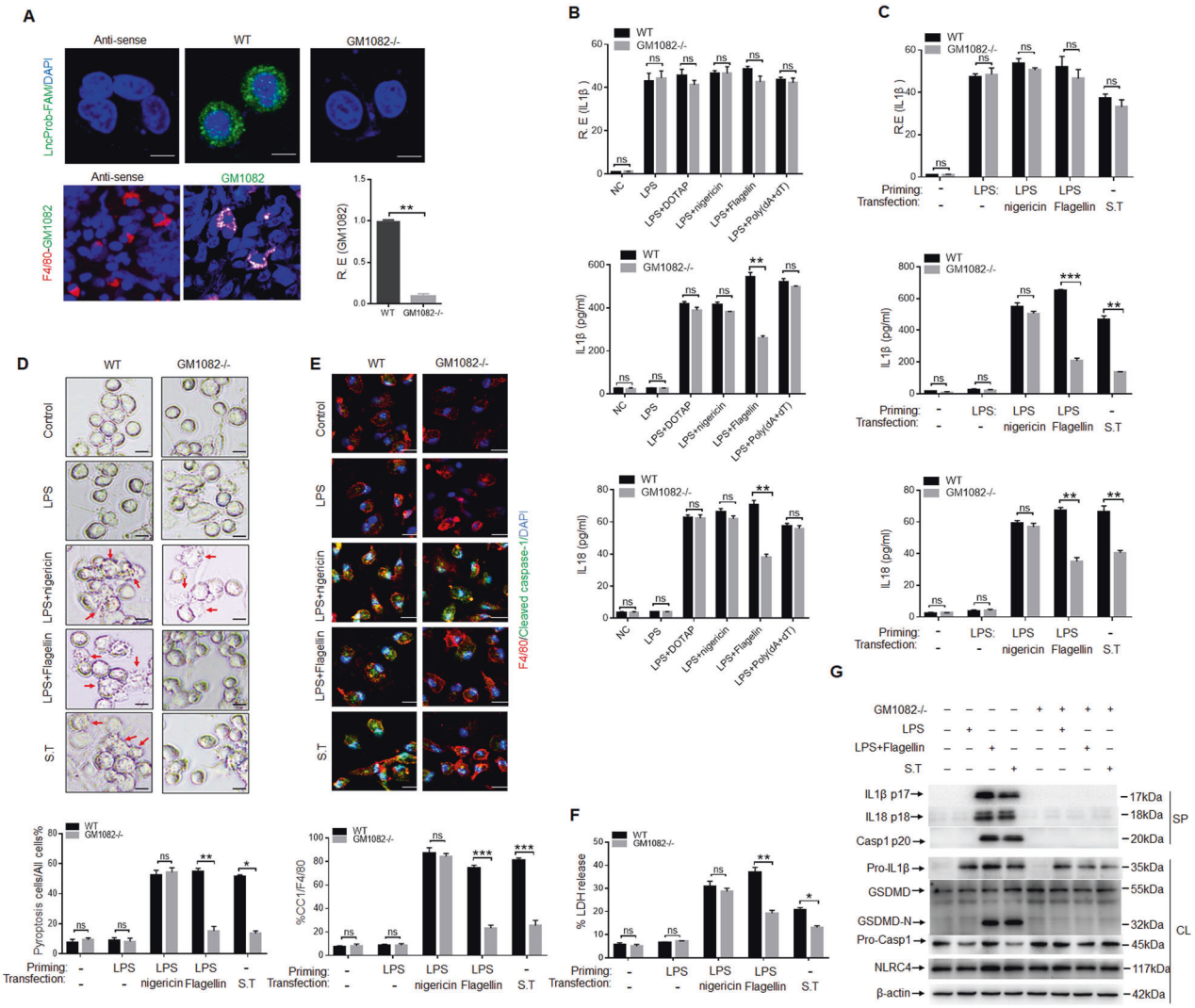

Fig. 5 *LNCGM1082* in human macrophages played a similar to that in mice. **A** Fluorescence in situ hybridization of *LNCGM1082* in the THP-1 monocyte/macrophage line and qRT–PCR of *LNCGM1082*−/− *THP-1* cells (upper) and macrophages from human colon tissues (lower). Red, F4/80; green, *LNCGM1082*; blue, nuclei. Scale bar, 2.5 μM. LNCGM1082−/−, *LNCGM1082*−/− macrophages. **B** qRT–PCR assay (upper) of IL-1β level and ELISAs (lower) of IL-1β and IL18 levels in the supernatants of wt and *LNCGM1082*−/− THP-1 cells, which had been stimulated by different stimuli. R.E., relative expression. **C** qRT–PCR assay (upper) of IL-1β level and ELISAs (lower) of IL-1β and IL18 levels in the supernatants of wt and *LNCGM1082*−/− THP-1 cells, which had been stimulated by LPS plus nigericin, flagellin or *S.* T. R.E., relative expression. **D** Images of THP-1 and *LNCGM1082*−/− THP-1 cells captured by light microscopy after stimulation with LPS plus nigericin, LPS plus flagellin or *S.* T. The arrows indicate pyroptotic cells. Scale bar, 5 μM. **E** Immunostained THP-1 and *LNCGM1082*−/− THP-1 cells after stimulation with LPS plus nigericin, LPS plus flagellin or *S.* T. **F** LDH in the supernatants of THP-1 cells stimulated with LPS plus nigericin, LPS plus flagellin or *S.* T. **G** Western blots showing proteins from THP-1 lysates and supernatants from cells stimulated with LPS plus flagellin or *S.* T. SP, supernatants; CL, cell lysates. Two-sided Student's *t* test was performed with the data shown in (**B**)–(**F**). n.s., not statistically significant; *, $p < 0.05$; **, $p < 0.01$; ***, $p < 0.001$

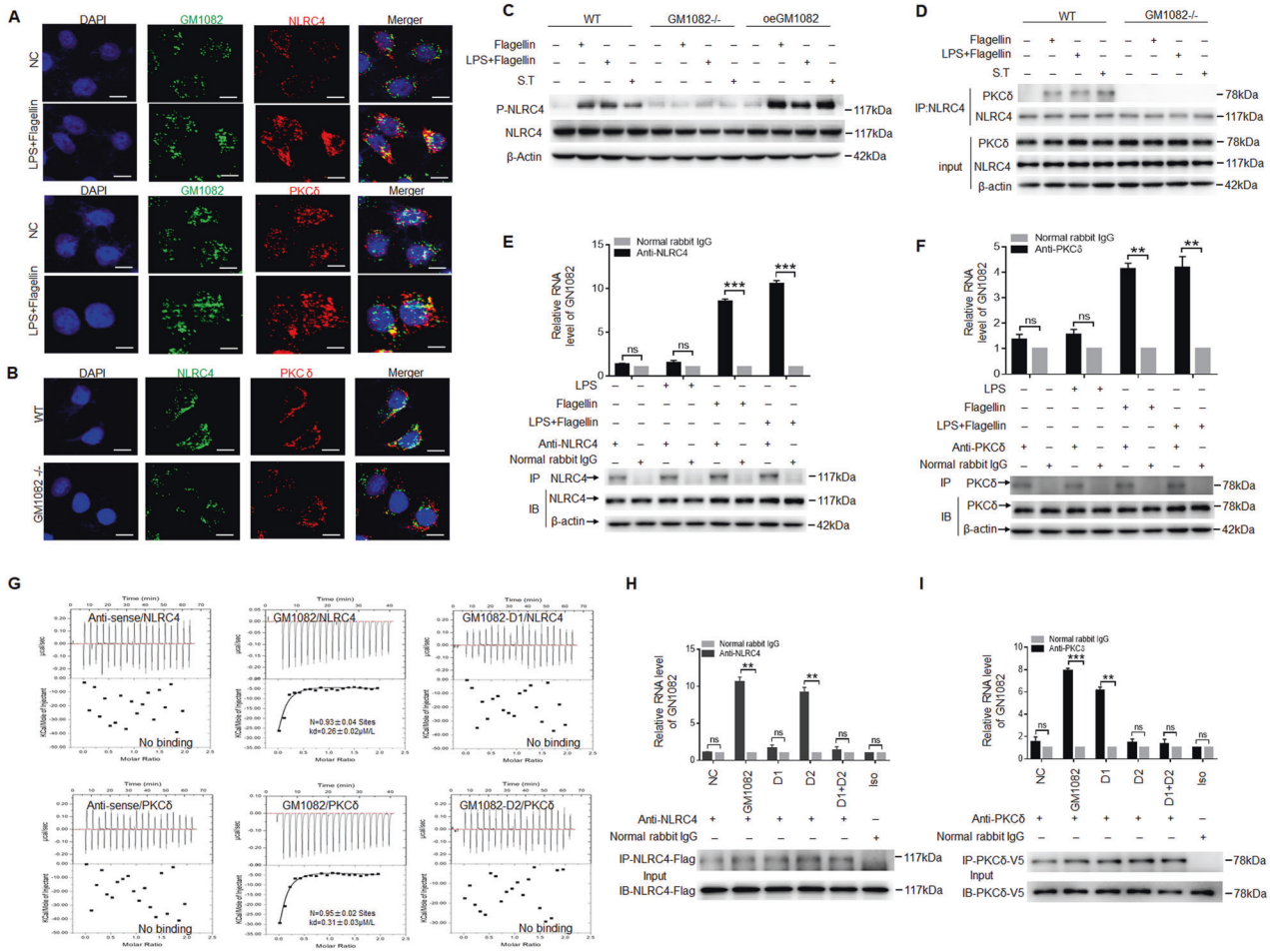

Fig. 6 Binding of human *LNCGM1082* with NLRC4 and PKCδ. **A** Immunostaining and RNA-FISH of NLRC4, PKCδ and *LNCGM1082* in THP-1 cells. Red, NLRC4 or PKCδ; green, *LNCGM1082*; blue, nuclei. Scale bar, 2.5 μM. **B** Immunostaining of NLRC4 and PKCδ in WT and *LNCGM1082*-KO THP-1 cells. Red, PKCδ; green, NLRC4; blue, nuclei. Scale bar, 2.5 μM. **C** Western blots showing phosphorylated NLRC4 in THP-1 cells after exposure to *S*. T or flagellin. **D** Immunoblot showing NLRC4 and PKCδ in THP-1 cells. Immunoprecipitation was performed using anti-NLRC4 antibodies, and then immunoblotting was performed using anti-PKCδ antibody. **E-F** RIP with THP-1 cells after to flagellin or *S*. T. Cell lysates were incubated with normal rabbit IgG, anti-NLRC4 antibody or anti-PKCδ antibody. The immunoprecipitates were analyzed by qRT–PCR to determine the *LNCGM1082* level. **G** ITC analysis of the binding of human *LNCGM1082* or mutated *LNCGM1082* (deletion of the NLRC4-binding site D1 or PKCδ-binding site D2) to NLRC4 and PKCδ. **H** RIP with Flag-tagged NLRC4 and *LNCGM1082*, *LNCGM1082* D1, *LNCGM1082* D2 or *LNCGM1082* D1/D2 cotransfected HEK293T cells. RIP was performed using anti-Flag antibody or an isotypic control (Iso). **I** RIP with V5-tagged PKCδ and *LNCGM1082*, *LNCGM1082* D1, *LNCGM1082* D2 or *LNCGM1082* D1/D2 cotransfected HEK293T cells. RIP was performed using anti-V5 antibody or an isotypic control (Iso). Two-sided Student's *t* test was performed with the data shown in E-F and H-I. n.s., not statistically significant; **, $p < 0.01$; ***, $p < 0.001$

genes, ARHGAP 33 or PRODH2, in human macrophages (Supplementary Fig. 2B, C). The effects of *LNCGM1082* deficiency identified in mouse macrophages were also observed in the *huLNCGM1082*−/− human macrophages, including reduced IL-1β and IL-18 maturation rates and resistance to pyroptosis after exposure to flagellins with LPS or *S*. T infection (Fig. 5B–G).However, similar *huLNCGM1082* roles were not observed in macrophages exposed to LPS with DOTAP, LPS with nigericin or LPS with poly (dA+dT) (Fig. 5B–G). These findings indicate that *huLNCGM1082* promotes IL-1β maturation and sensitivity to pyroptosis, similar to the effect of mouse *LNCGM1082* on human macrophages.

Human NLRC4 activation requires *LNCGM1082*

Since human and mouse *LNCGM1082* exhibited similar functions in macrophages, we analyzed these lncRNAs using bioinformatics. The NLRC4- and PKCδ-binding motifs are similar in both human *huLNCGM1082* and mouse *LNCGM1082* (Supplementary Fig. 13A). We used SWISS-MODEL software to model the protein crystal structure of NLRC4 and PKCδ in humans and mice. The crystal structures of NLRC4 and PKCδ in humans and mice were similar (Supplementary Fig. 13B, C). All of these results suggest that *huLNCGM1082* may undergo binding with NLRC4 and PKCδ in a manner similar to *LNCGM1082* in mice Indeed, marked binding of NLRC4 and PKCδ was observed in THP-1 human macrophages, whereas NLRC4 and PKCδ did not bind in *huLNCGM1082*−/− THP-1 cells exposed to LPS with flagellin (Fig. 6A, B), which was similar to mouse the findings observed with *LNCGM1082*−/− macrophages. NLRC4 phosphorylation in *huLNCGM1082*−/− macrophages was not evident after exposure to flagellin or *S*. T (Fig. 6C). *HuLNCGM1082* exhibited binding with NLRC4 and PKCδ as indicated by IP and RIP (Fig. 6D–F). These binding events were confirmed by ITC (Fig. 6G). The data also confirmed that the *LNCGM1082* D1 region was critical for binding with NLRC4, whereas D2 mediated the binding of *LNCGM1082* with PKCδ (Fig. 6G–I). These data show that *huLNCGM1082* can bind with NLRC4 and PKCδ in human macrophages.

TLR5 mediates the expression of *LNCGM1082*

Finally, we investigated the underlying regulatory mechanism that directs the expression of *LNCGM1082*. When we analyzed the expression of genes in gut tissues after *S.* T infection, the expression of *LNCGM1082* was markedly increased (Supplementary Fig. 14), suggesting that *LNCGM1082* expression may be related to *S.* T infection. Therefore, we analyzed *LNCGM1082* after exposure to *S.* T or bacterial flagellin, key effector molecules that not only trigger cytosolic sensors but also bind and activates membrane-bound TLR5 [36, 37]. The data showed that both *S.* T and flagellin induced the expression of *LNCGM1082* in mouse macrophages but not in *TLR5*−/− macrophages (Fig. 7A–C). Furthermore, both *S.* T and flagellin induced *LNCGM1082* expression in a dose- and time-dependent manner (Fig. 7A–C and Supplementary Fig. 15A-F). TLR5 is expressed in human THP-1 macrophages [38]. Both *S. T* and flagellin induced *LNCGM1082* expression in THP-1human macrophage s (Fig. 7D, E). Notably, this expression was rapidly detected after exposure to *S.* T (Fig. 7A, D). *S.* T- and flagellin-mediated effect on *LNCGM1082* expression depended on TLR5, MyD88, IRAK1, IRAK4 and NF-κB (Supplementary Fig. 15G-J). In addition, NLRC4 did not bind with PKCδ in *TLR5*−/− macrophages exposed to LPS with flagellin (Fig. 7F), implying that *LNCGM1082* is note expressed in *TLR5*−/− macrophages. However, the binding of PKCδ to NLRC4 and the phosphorylation of NLRC4 were rescued by the overexpression of *LNCGM1082* in *TLR5*−/− macrophages (Fig. 7G, H). Taken together, these data indicate that TLR5 induces *LNCGM1082* in both human and mouse macrophages.

DISCUSSION

In this study, we report an important physiological role for host *LNCGM1082* against *S.* T infection. *LNCGM1082* deficiency causes a reduced mature Il-1β level and pyroptosis rate in macrophages. *LNCGM1082*−/− mice are highly sensitive to *S.* T infection. Mechanistically, activation of NLRC4 requires *LNCGM1082*, which binds with PKCδ and NLRC4 to induce the phosphorylation of NLRC4. This mechanism suggests that the interaction of certain intracellular kinases with their substrates require lncRNAs. A similar phenomenon has been observed by other researchers [39–43]. For example, the lncRNA HULC directly binds to two glycolytic enzymes, lactate dehydrogenase A and pyruvate kinase M2, to promote phosphorylation [42]; the *LINK-A lncRNA* facilitates the recruitment of BRK to the EGFR:GPNMB complex and BRK kinase activation [40]; and *LNCRNAAK023948* is required for the interaction between DHX9 and p85 to enhance p85 stability and promote AKT activity [43]. We also demonstrated that *LNCGM1082* expression can be rapidly induced by *S. T* through TLR5. Since inflammasome NLRC4 activation generally requires a long time (~4 h) and is a key process mediated by Toll-like receptor ligands [8, 44, 45], the rapid expression of TLR5-mediated *LNCGM1082* may be important for switching or promoting the activation of NLRC4 by *S.* T, which induces inflammation and eliminates bacteria (Fig. 7I). In addition, our results suggest that *LNCGM1082* is involved in NLRC4 activation induced by other bacteria that possess flagella.

The activation of NLRC4 is an important event during NLRC4 inflammasome activation. Biochemical, structural and genetic studies have established that activation of NLRC4 requires NAIPs (NAIP1, NAIP2, NAIP5, and NAIP6) in C57BL/6 mice, where they act as sensors to detect bacterial flagellin, T3SS needles or rod proteins [46]. NLRC4 is also transcriptionally induced by interferon regulatory factor (IRF)8 [44]. IRF8 is as a transcriptional activator of murine NAIP1, 2, 5, and 6 and NLRC4. NLRC4 undergoes posttranslational modifications that can regulate its assembly and function [8, 9, 12]. Previous work with murine macrophages led to the identification of NLRC4 phosphorylation by PKCδ in response to *S.* T [8]. Furthermore, this modification is required for NLRC4 inflammasome assembly [8]. NLRC4 interacts directly with infection-induced NLRP3, which then recruits ASC and activates caspase-1 [47]. Activated NLRC4 also undergoes substantial structural reorganization and interacts with and activates other quiescent NLRC4 molecules to ultimately form a complex with a 10- to 12-spoke wheel- or disk-like architecture [48, 49]. Notably, the importance of PKCδ binding and phosphorylation of NLRC4 to its inflammasome activity will be determined in subsequent work. For example, LRRK2 was been shown to phosphorylate NLRC4 [47]. Both *S.* T and *S. flexneri* induce the activation of the NLRC4 inflammasome independent of PKCδ [50].

LncRNAs are involved in numerous important biological processes [15, 16]. We demonstrate that *LNCGM1082* binds with PKCδ and NLRC4 to induce the phosphorylation of NLRC4. Other studies have reported that cytoplasmic lncRNAs participate in regulating protein stability and modification [51, 52].

MATERIALS AND METHODS

The sources and identifiers of all key reagents and resources are listed in Supplementary Table 1 in the Supplementary Materials.

Mice and cell lines

LNCGM1082-deficient mice with a C57BL/6J background were generated by the Model Animal Research Center of Nanjing University (Nanjing, Jiangsu, China) using the CRISPR–Cas9 system. Cas9 mRNA and sgRNA were coinjected into zygotes, and sgRNA-directed Cas9 endonuclease cleavage upstream of E1 and downstream of E2 was performed to create a DSB (double-strand break). These breaks were repaired by nonhomologous end joining (NHEJ) and resulted in the deletion of the Arhgap33 gene (*LNCGM1082*). *Caspase1/11*−/− and *NLRC4*−/− mice were obtained from Prof. Shao, National Institute of Biological Sciences, Beijing; *NLRP3*−/− mice were obtained from Prof. Meng, Pasteur Institute, Shanghai; *TLR5*−/− mice were obtained from Institute of Model Animal, Wuhan University; C57BL/6 and B6. SJL-CD45a(Ly5a) (CD45.1) mice were purchased from the Model Animal Research Center of Nanjing University (Nanjing, Jiangsu, China). All the mice were maintained under specific-pathogen-free conditions at the Animal Center of Nankai University. All animal experiments were carried out in accordance with the Nankai University Guide for the Care and Use of Laboratory Animals. The HEK293T human embryonic kidney cell line was obtained from the American Type Culture Collection.

Mouse models

For *S.* T infection, a *Salmonella* infection model was established according to a previous method [53]. Briefly, water and food were denied for 4 h before oral gavage treatment of the mice with 7.5 mg of streptomycin. Twenty hours after streptomycin treatment, water and food were again withdrawn, and then, the mice were infected with *S.* T (200 CFUs). Mice were weighed every other day to determine the percentage of weight change, which was calculated as follows: % weight change = (weight at Day X-Day 0/weight at Day 0) × 100. The mice were sacrificed on the indicated days, and histological studies were performed. Representative colon and lung tissues were embedded in paraffin for hematoxylin/eosin (H&E) staining, embedded in OCT compound and frozen with liquid nitrogen for subsequent immunostaining. The lung, liver, and spleen were collected and then homogenized for 2 min in PBS with metal beads by using a TissueLyser II apparatus. CFUs were quantified by plating lysates onto LB agar followed by incubation overnight.

For establishing an *E. coli* 0160-labeled GFP infection model, mice were treated with panantibiotics (ampicillin (A, 1 g/L), vancomycin (V, 0.5 g/L), neomycin sulfate (N, 1 g/L), and metronidazole (M, 1 g/L)) in drinking water for one week. To confirm the elimination of bacteria, stool was collected from antibiotic-treated and untreated mice and cultured under anaerobic and aerobic conditions. After confirming the elimination of bacteria, the mice were gavaged using 1×10^9 CFU *E. coli*. After two days, the colon and feces were collected, and CFUs were quantified by plating lysates onto LB agar followed by incubation overnight.

For determining the chronic toxicity induced by LPS, mice were intraperitoneally injected with 20 mg/kg LPS (O111:B4), and then, serum IL1β and IL18 concentrations were measured. For an acute toxicity experiment, mice were injected with 52 mg/kg LPS, and then, survival (time to moribund) was measured.

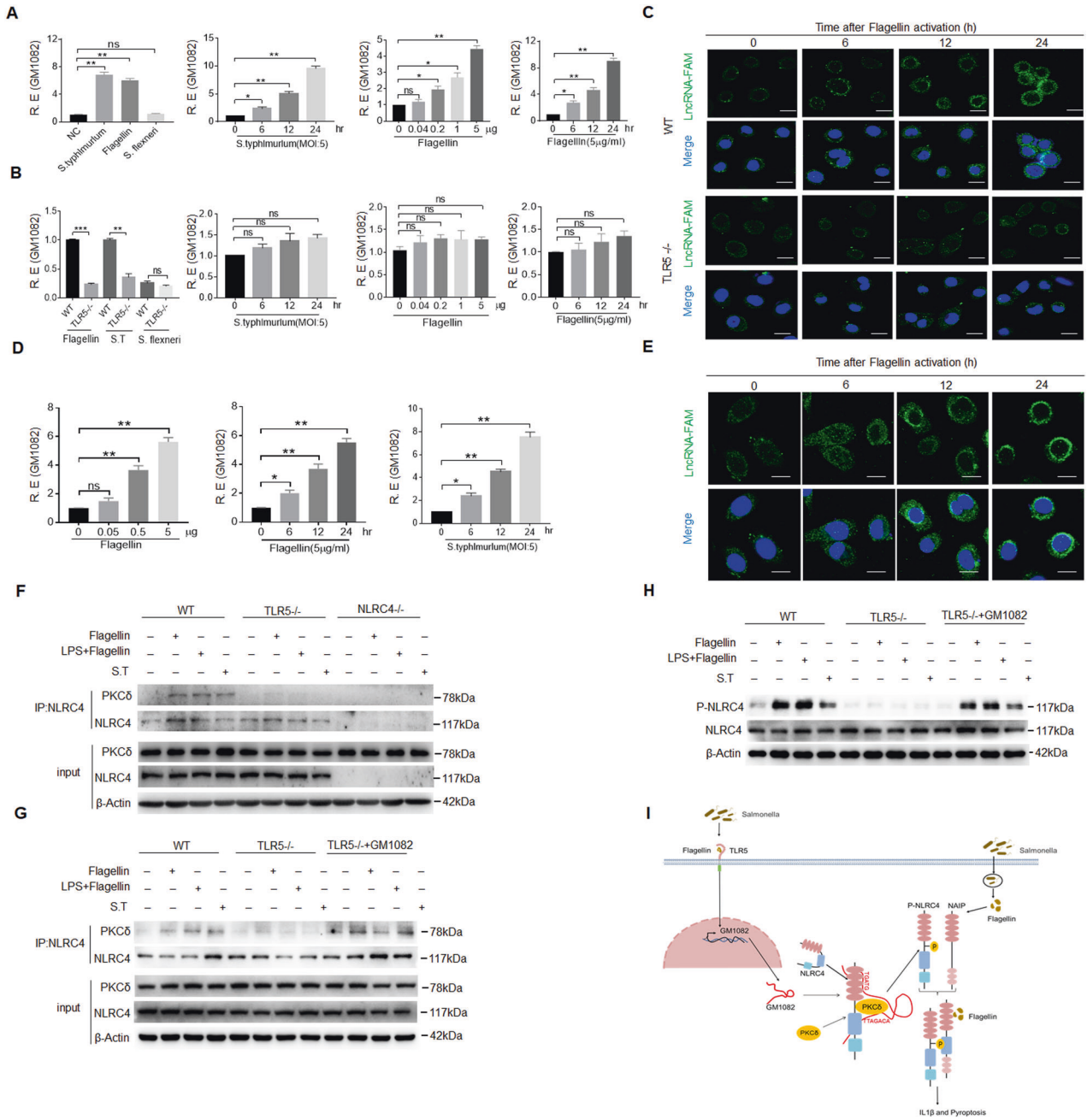

Fig. 7 Flagellin induced *LNCGM1082* mediated through TLR5 action in macrophages. **A** qRT–PCR assay of *LNCGM1082* level in macrophages stimulated with flagellin, *S.* T and *S. flexneri*, a nonflagellated bacterium or *S. T* for different durations or with flagellin at different concentrations and for different durations. **B** qRT–PCR of *LNCGM1082* in WT and *TLR5−/−* macrophages after exposure to flagellin, *S.* T and *S. flexneri* or *S.* T for different durations or flagellin at different concentrations for different durations. **C** RNA-FISH of *LNCGM1082* in wt and *TLR5−/−* macrophages after exposure to flagellin for different durations. Green, *LNCGM1082*; blue, nuclei. Scale bar, 2.5 μM. **D** qRT–PCR assay of *LNCGM1082* level in THP-1 cells after exposure to different concentrations of flagellin for different durations or *S.* T for different durations. **E** RNA-FISH of *LNCGM1082* in THP-1 cells after exposure to flagellin for different durations. Green, *LNCGM1082*; blue, nuclei. Scale bar, 2.5 μM. **F** Immunoblot showing NLRC4 and PKCδ in wt, TLR5−/− and NLRC4−/− macrophages. Immunoprecipitation was performed using anti-NLRC4 antibodies, and then, immunoblotting was performed using anti-PKCδ antibody. **G** Immunoblot showing NLRC4 and PKCδ in wt, *TLR5−/−* and exogenous LNCGM1082-transduced TLR5−/− macrophages. Immunoprecipitation was performed using anti-NLRC4 antibody, and then, immunoblotting was performed using anti-PKCδ antibody. **H** Immunoblots showing phosphorylated NLRC4 in wt, *TLR5−/−* and exogenous LNCGM1082-transduced TLR5−/− macrophages after exposure to *S.* T or flagellin. **I** Mechanism by which *LNCGM1082* induced by *S.* T regulated the activation of NLRC4. R.E., relative expression. Two-sided Student's *t* test was performed with the data shown in (**A**), (**B**) and (**D**); n.s., not statistically significant; *, $p < 0.05$; **, $p < 0.01$; ***, $p < 0.001$

For bone marrow cell (BMC) transplantation experiments, BMCs collected from wt or *LNCGM1082−/−* mice were injected into different recipient mice, which had been irradiated (800 cGy, a single dose) using a Shepherd Mark I Cesium Irradiator (J.L. Shepherd and Associates). After 3 weeks, *S.* T was introduced into the recipient mice.

Preparation of macrophage and other cell cultures

Macrophages were generated in the peritoneal cavity of mice after intraperitoneal injection with 4 mL of 3% thioglycollate medium. After four days, 5 mL of cold phosphate-buffered saline (PBS) containing 3% FBS was injected into the peritoneal cavity. Following this injection, gentle massage

was performed, and peritoneal fluid was subsequently isolated and removed. Next, the cells derived from the peritoneal washing fluid were seeded at 2×10^6 in RPMI containing 10% FBS. Nonadherent cells were removed 4 h after seeding by extensive washing with medium. Cone marrow-derived macrophages (BMDMs) were obtained from the bone marrow of the tibia and femur, cultured in DMEM with 10% FBS, 20 ng/ml mouse M-CSF, and 1% penicillin/streptomycin for 6 d and then replated and used for experiments. HEK293T cells were cultured in DMEM containing 10% FBS, 1% penicillin, and streptomycin.

MicroRNA transfection and shRNA- or LNCGM1082-carrying lentivirus construction and transduction

Peritoneal macrophages were transfected with microRNAs using HiPerFect transfection reagent according to the manufacturer's instructions. A short hairpin RNA (shRNA) target sequence was chosen with BLOCK-iT™ RNAi Designer (Invitrogen) and/or by i-Score Designer 38. The shRNA or *LNCGM1082* constructs were made using a pGreenPuro™ cloning and expression lentivector kit according to the manual. The negative control was luciferase RNA in the kit. For packaging lentivirus particles, an shRNA or *LNCGM1082* lentivector together with pMD2.G and psPAX2 packaging plasmids were cotransfected into 293T cells. Peritoneal macrophages were infected with the lentiviral supernatants in the presence of 8 μg/ml polybrene via centrifugation and then cultured with complete medium for 24 h.

Ex vivo stimulation

For activation of Toll-like receptors, BMDMs were stimulated with concentrations of Pam3CSK4 (50 nM, TLR 1/2), poly(I:C) (10 μg/ml, TLR3), LPS (2 μg/ml, TLR4), flagellin (5 μg/ml, TLR5), FSL-1 (50 ng/ml, TLR2/6), R848 (5 μg/ml, TLR7/8), and ODN 1585 (5 μM, TLR9) for 12 h.

For inflammasome activation, peritoneal macrophages were primed with LPS (2 μg/mL) for 4 h and subsequently stimulated with nigericin (5 μM) for 0.5 h to activate the NLRP3 inflammasome, DOTAP-transfected LPS (2 μg/mL) for 3 h to activate caspase 11, DOTAP-transfected flagellin (5 μg/mL) for 3 h to activate the NLRC4 inflammasome, and Lipofectamine 2000-transfected poly (dA:dT) (1 μg/mL) for 3 h to activate the AIM2 inflammasome. Total cell lysates and supernatants were analyzed by immunoblotting.

For stimulation in vitro, *S*. T or *Shigella flexneri*, a nonflagellated bacterium, was grown in Luria–Bertani medium at 37 °C overnight. Bacteria were added to macrophages at a multiplicity of infection (MOI) of 5 and cultured for 3 h, and total cell lysates and precipitated supernatants were analyzed by immunoblotting.

Lentiviruses and plasmid construction

LNCGM1082 shRNA targets were chosen from the target sequences produced with BLOCK-iT™ RNAi Designer (Invitrogen) and/or by i-Score Designer. The shRNA constructs were made using a pGreenPuro™ shRNA Cloning and Expression Lentivector kit according to the manual. The shNC was the luciferase shRNA in the kit. For packaging lentiviral particles, the shRNA lentivector together with pMD2G and psPAX2 packaging plasmids were cotransfected into 293T cells.

For preparation of plasmids, the sequences of mouse NLRC4, including NA-LRR, LRR, ΔLRR, CARD-NA, mouse PKCδ, human NLRC4, human PKCδ, mouse/human *LNCGM1082*, mouse *arhgap33os-202* and Open Reading Frame 2 or 3 in mouse *LNCGM1082*, were amplified using PCR. The PCR products were cloned into a pcDNA™3.1/V5-His TOPO® TA plasmid. After sequencing, plasmid constructs were used to transfect HEK293T cells.

RNA extraction and qRT–PCR assays

Total RNA was extracted from the cells, tissues and organs using TRIzol reagent. First-strand cDNA was generated from total RNA using oligo-dT/random primer mix and reverse transcriptase. Quantitative real-time PCR (qRT–PCR) was conducted using QuantiTect SYBR Green PCR Master Mix and specific primers in an ABI Prism 7000 analyzer (Applied Biosystems). GAPDH mRNA expression was detected in each experimental sample as the endogenous control. Fold changes were calculated using the ΔΔCt method according to the analyzer manufacturer's instructions (Applied Biosystems). All reactions were performed in triplicate.

Northern blotting

For Northern blotting, total harvested RNA was separated on a 1% agarose formaldehyde gel and then transferred to a Hybond nylon membrane via Trans-Blot SD semidry electrophoretic transfer. The membrane was prehybridized for 1 h at 42 °C and incubated with a probe overnight at the same temperature. After washing, the membrane was blocked and incubated with digoxin antibody conjugated to HRP.

Western blotting

For Western blotting, our previously described method [54] was used in this study. Briefly, cells were harvested at the indicated times and rinsed twice with ice-cold PBS. Cell extracts were prepared with lysis buffer and centrifuged at $13{,}000 \times g$ for 10 min at 4 °C. Protein samples were electrophoresed on 12% polyacrylamide gels and transferred to PVDF membranes. After the membranes were blocked with 5% skim milk powder for 1 h at room temperature, they were incubated with primary antibody in TBST overnight at 4 °C. Secondary antibodies conjugated to horseradish peroxidase (HRP) (1:10000) were labeled as described to our previous study. The signals were captured on by autoradiography film and measured when HRP substrate was added to the membranes.

Cytosolic and nuclear fractionation

The indicated cells were incubated with hypotonic buffer (25 mM Tris-HCl, pH 7.4; 1 mM MgCl2; and 5 mM KCl) on ice for 5 min. An equal volume of hypotonic buffer containing 1% NP-40 was then added, and each sample was incubated on ice for another 5 mins. After centrifugation at $5000 \times g$ for 5 min, the supernatant was collected as the cytosolic fraction. The pellets were resuspended in nucleus resuspension buffer (20 mM HEPES, pH 7.9; 400 mM NaCl; 1 mM EDTA; 1 mM EGTA; 1 mM DTT; and 1 mM PMSF) and incubated at 4 °C for 30 min. The nuclear fraction was collected after removing insoluble membrane debris by centrifugation at $12{,}000 \times g$ for 10 min.

H&E staining

For hematoxylin/eosin (H&E) staining, previously reported methods were followed [54]. Briefly, lung tissues were fixed in 4% (w/v) paraformaldehyde in buffered saline and embedded in paraffin, and 5-μm colon sections were cut and stained with H&E.

Cell isolation and flow cytometry

For the staining of lamina propria (LP) lymphocytes, the colon was isolated and cleaned by shaking the samples in ice-cold PBS four times before the tissues were cut into 1-cm pieces. The epithelial cells were removed by incubating the tissue in HBSS with 2 mM EDTA for 30 mins with shaking. The LP cells were isolated by incubating the tissues in digestion buffer (DMEM, 5% fetal bovine serum, 1 mg/ml collagenase IV and DNase I) for 40 min at 37 °C with shaking. The digested tissues were then pressed through a 40-mm filter. Cells were resuspended in 10 ml of the 40% fraction of a 40:80 Percoll gradient, which was overlaid on 5 ml of the 80% fraction in a 15-ml Falcon tube. Percoll gradient separation was performed by centrifugation for 20 min at 1800 rpm at room temperature. LP cells were collected at the interphase of the Percoll gradient, washed and resuspended in medium, and then stained and analyzed by flow cytometry. Dead cells were eliminated after detection with 7-AAD staining.

LNCGM1082 deletion in human macrophages

In brief, we first analyzed the target gene sequence, screened suitable target sites, and designed one sgRNA for each target site. According to the designed sgRNA sequence, oligo DNA was synthesized. The empty vector was digested with the Cas9 gene (with a fluorescent tag (GFP) and screening gene (puromycin)) to obtain a linearized plasmid. Oligo DNA was mixed with a linearized empty vector, ligated with T4 ligase and incubated overnight at 16 °C. The verified plasmid was amplified, cultured, and extracted. THP-1 cells were seeded in 12-well plates at a density of 100,000 cells per well. After 24 h, the cells were transiently transfected with 4 μg of the Cas9 plasmid using Lipofectamine 2000. After 24 h of transfection, puromycin was added at a final concentration of 3 μg to the culture dish for screening. After 3 days, the cells were diluted to a density of 1-2 cells/200 μl in 40 mL of complete growth medium, and the cells were plated in a 96-well plate. After 5 days, the 96-well plate was observed under an optical microscope, and the wells containing single cells were marked. When the cell density reached 70%~90%, the cell genome was extracted and amplified with previously designed PCR primers, and the amplified products were sequenced.

Immunostaining and RNA-FISH

Immunostaining and RNA fluorescence in situ hybridization (RNA-FISH) were performed according to previously reported protocol [55]. Briefly, cells were first spread onto sterile and 0.01% poly-lysine-treated slides at the bottom of 6-well tissue culture dishes. Then, the slides were processed sequentially with ice-cold CSK buffer, CSK + 0.4% Triton X-100 buffer and CSK buffer for 30 s to induce cell membrane perforation. The slides were then treated with 4% PFA for 10 min and then with cold 70% ethanol three times for cell fixation. After rinsing three times with ice-cold PBS, the slides were blocked in prewarmed 5% goat serum for 30 min at 37 °C. Then, the slides were incubated with primary antibody at 37 °C for 1 h, washed three times with 1 × PBS/0.2% Tween-20 for 3 min on a rocker, and then incubated with secondary antibody at 37 °C for 30 min. The slides were dehydrated by moving them through an ethanol series (85, 95, and 100% ethanol) at room temperature for 2 min each in each gradient, air-dried at room temperature for 15 min, and finally hybridized using the indicated probes overnight at 37 °C in a humidified chamber. After washing with 2× SSC/50% formamide, 2× SSC, and 1× SSC three times, DAPI dye was added. Finally, the slides were sealed and observed using a confocal microscope.

RNA Immunoprecipitation (RIP)

RNA immunoprecipitation was performed according to a previously reported protocol [19]. Briefly, the cells were harvested, washed, added to ice-cold IP lysis buffer containing 0.5% ribonuclease inhibitor, and incubated on ice for 5 min with periodic mixing. Then, the lysates were transferred into a microcentrifuge tube and centrifuged at 13,000 × *g* for 10 min to pellet the cell debris at 4 °C. The supernatants were transferred into a new tube, and protein G agarose was added and incubated for 1 h at 4 °C with rotation for preclearing. Immunoprecipitating antibody was added and incubated overnight at 4 °C with rotation. Protein G agarose was pelleted by brief centrifugation (3000 × *g* for 1 min) and then washed sequentially with IP lysis buffer (containing 0.5% ribonuclease inhibitor). Finally, RNA was extracted from protein/RNA complexes on the beads using TRIzol reagent. The RNA was dissolved in DEPC-water and quantified by quantitative PCR (qPCR).

UV-RIP

The cells were incubated for 12 h with 100 mM 4-thiouridine (4-SU) and then cross-linked with a CL-1000 Ultraviolet Crosslinker (UVP) and 365 nm UV light. Cells were lysed, and the lysates were immunoprecipitated with primary antibody or isotypic antibody. RNase T1 (final concentration 50 U/mL) was added, and then, the beads were washed with high-salt wash buffer (50 mM HEPES-KOH, pH 7.5; 500 mM KCl; 0.05% (v/v) NP40;0.5 mM DTT; and protease inhibitor cocktail). In preparation for UV-RIP-seq, the protein–RNA complex was treated with proteinase K. Immunoprecipitated RNA was purified using acidic phenol, and the RNA was subjected to high-throughput sequencing with a HiSeq 4000 system following the PE100 strategy. For RIP-qPCR analysis, the primers used are listed in Table S1. The amount of immunoprecipitated RNA is presented as the percentile of input RNA (% input).

Individual-nucleotide resolution cross-linking and immunoprecipitation (iCLIP)

The cells were first subjected to crosslinking with 0.15 J/cm^2 of 254 nm UV light in a crosslinker HL-2000 (UVP), lysed with NP-40 lysis buffer on ice for 10 min, and treated with RNase A (200 ng/ml) for 5 min. Clear lysates were incubated with anti-NLRC4 or isotypic antibody overnight at 4 °C. After immunoprecipitation, the beads were incubated with a biotin-labeled linker. After being separated on a 4–12% NuPAGE gel, the protein–RNA complexes were transferred to an nitrocellulose membrane. Biotin-labeled RNA was detected and visualized according to the instructions of a chemiluminescent kit. Visualized protein–RNA complexes were cut from the membrane corresponding to the size of NLRC4. RNA was isolated from solution with phenol–chloroform and subjected to library construction.

Immunoprecipitation

Immunoprecipitation (IP) was performed according to our previously described method [19]. The cells were lysed in IP lysis buffer containing 10% PMSF. Protein A/G magnetic beads were first added to the cell lysates for preclearing. The supernatants were collected after centrifugation at 12,000 rpm and then immunoprecipitated overnight at 4 °C with the indicated antibodies. Protein A/G magnetic beads were added to the cell lysate and incubated for an additional 3 h. After being washed with IP lysis buffer five times, Protein A/G magnetic beads were denatured, and the proteins were resolved by SDS–PAGE gels.

RNA–protein pull-down analyses

RNA–protein pull-down analyses were performed using a Pierce™ Magnetic RNA–Protein Pull-Down Kit. Transfected and induced cells were harvested, and cell lysates were prepared using IP lysis buffers. *LNCGM1082* and mutants were transcribed and labeled using an RNA 3´ Desthiobiotinylation Kit in vitro. Fifty microliters of beads and 50 pmol labeled RNA were added to RNA capture buffer and incubated for 30 min at room temperature with agitation to bind labeled LNCGM1082 to streptavidin magnetic beads. After washing the beads with an equal volume of 20 mM Tris (pH 7.5), 100 µL of protein–RNA binding buffer was added to the beads and thoroughly mixed. One hundred microliters of master mix to induce the RNA–protein binding reaction was added to the RNA-bound beads and mixed by pipetting. The beads were then incubated for 60 min at 4 °C with rotation to bind RNA-binding proteins to RNA. After washing the beads with 100 µl of washing buffer twice, 50 µL of elution buffer was added and incubated for 30 min at 37 °C with agitation. The samples were analyzed on a gel.

Isothermal titration calorimetry measurements

Calorimetric experiments were conducted at 25 °C with a MicroCal iTC200 instrument. The NLRC4 and PKCδ proteins were dialyzed against titration buffer containing 20 mM Tris-HCl, pH 7.4; 150 mM NaCl; and 2 mM $MgCl_2$. Lyophilized RNA samples were prepared in titration buffer, renatured at 95 °C for 2 min, 4 °C for 2 min and 25 °C for 20 min, and then diluted to the required concentration for ITC titration. The calorimetric titration data were analyzed using Origin 7.0 software based on the "One Set of Sites" fitting model.

Statistical analyses

Two-sided Student's *t* tests and one-way ANOVA Bonferroni's multiple comparison tests were performed to determine the significance of differences. The statistical significance of survival curves was estimated using the Kaplan–Meier method, and the curves were compared by generalized Wilcoxon's test. These analyses were performed withy GraphPad Prism 5 software (GraphPad Software). A 95% confidence interval was considered significant and is presented as $p < 0.05$.

DATA AVAILABILITY

Data from the microarray are available through the GEO database (Supplementary Fig. 3: Accession Number: GSE221313; Supplementary Fig. 9A: Accession Number: GSE173399; and Supplementary Fig. 14A, Accession Number: GSE173398).

REFERENCES

1. Kay C, Wang R, Kirkby M, Man SM. Molecular mechanisms activating the NAIP-NLRC4 inflammasome: Implications in infectious disease, autoinflammation, and cancer. Immunol Rev. 2020;297:67–82.
2. Duncan JA, Canna SW. The NLRC4 Inflammasome. Immunol Rev. 2018;281:115–23.
3. Lamkanfi M, Dixit VM. Mechanisms and functions of inflammasomes. Cell. 2014;157:1013–22.
4. Rathinam VA, Fitzgerald KA. Inflammasome complexes: emerging mechanisms and effector functions. Cell. 2016;165:792–800.
5. Zhao Y, Yang J, Shi J, Gong YN, Lu Q, Xu H, et al. The NLRC4 inflammasome receptors for bacterial flagellin and type III secretion apparatus. Nature. 2011;477:596–600.
6. Grohmann E, Christie PJ, Waksman G, Backert S. Type IV secretion in Gram-negative and Gram-positive bacteria. Mol Microbiol. 2018;107:455–71.
7. Zhao Y, Shao F. The NAIP-NLRC4 inflammasome in innate immune detection of bacterial flagellin and type III secretion apparatus. Immunol Rev. 2015;265:85–102.
8. Qu Y, Misaghi S, Izrael-Tomasevic A, Newton K, Gilmour LL, Lamkanfi M, et al. Phosphorylation of NLRC4 is critical for inflammasome activation. Nature. 2012;490:539–42.
9. Liu W, Liu X, Li Y, Zhao J, Liu Z, Hu Z, et al. LRRK2 promotes the activation of NLRC4 inflammasome during Salmonella Typhimurium infection. J Exp Med. 2017;214:3051–66.

10. Koh EH, Yoon JE, Ko MS, Leem J, Yun JY, Hong CH, et al. Sphingomyelin synthase 1 mediates hepatocyte pyroptosis to trigger non-alcoholic steatohepatitis. Gut. 2021;70:1954–64.
11. Yang F, Yang Y, Zeng W. Blockade of anti-dsDNA ameliorates systemic lupus erythematosus in MRL/Faslpr mice through ameliorating inflammation via the PKCdelta-NLRC4 axis. Biochem Cell Biol. 2021;99:313–21.
12. Raghawan AK, Sripada A, Gopinath G, Pushpanjali P, Kumar Y, Radha V, et al. A disease-associated mutant of NLRC4 shows enhanced interaction with SUG1 leading to constitutive FADD-dependent caspase-8 activation and cell death. J Biol Chem. 2017;292:1218–30.
13. Derrien T, Johnson R, Bussotti G, Tanzer A, Djebali S, Tilgner H, et al. The GENCODE v7 catalog of human long noncoding RNAs: analysis of their gene structure, evolution, and expression. Genome Res. 2012;22:1775–89.
14. Ulitsky I, Bartel DP. lincRNAs: genomics, evolution, and mechanisms. Cell. 2013;154:26–46.
15. Rinn JL, Chang HY. Genome regulation by long noncoding RNAs. Annu Rev Biochem. 2012;81:145–66.
16. Ponting CP, Oliver PL, Reik W. Evolution and functions of long noncoding RNAs. Cell. 2009;136:629–41.
17. Anderson KM, Anderson DM, McAnally JR, Shelton JM, Bassel-Duby R, Olson EN. Transcription of the non-coding RNA upperhand controls Hand2 expression and heart development. Nature. 2016;539:433–6.
18. Kopp F, Mendell JT. Functional classification and experimental dissection of long noncoding RNAs. Cell. 2018;172:393–407.
19. Gao Y, Sun W, Shang W, Li Y, Zhang D, Wang T, et al. Lnc-C/EBPbeta negatively regulates the suppressive function of myeloid-derived suppressor cells. Cancer Immunol Res. 2018;6:1352–63.
20. Zhang P, Cao L, Zhou R, Yang X, Wu M. The lncRNA Neat1 promotes activation of inflammasomes in macrophages. Nat Commun. 2019;10:1495.
21. Broz P, Dixit VM. Inflammasomes: mechanism of assembly, regulation and signalling. Nat Rev Immunol. 2016;16:407–20.
22. Rathinam VAK, Zhao Y, Shao F. Innate immunity to intracellular LPS. Nat Immunol. 2019;20:527–33.
23. Sharif H, Wang L, Wang WL, Magupalli VG, Andreeva L, Qiao Q, et al. Structural mechanism for NEK7-licensed activation of NLRP3 inflammasome. Nature. 2019;570:338–43.
24. Zhang Z, Yuan B, Bao M, Lu N, Kim T, Liu YJ. The helicase DDX41 senses intracellular DNA mediated by the adaptor STING in dendritic cells. Nat Immunol. 2011;12:959–65.
25. Broz P, Newton K, Lamkanfi M, Mariathasan S, Dixit VM, Monack DM. Redundant roles for inflammasome receptors NLRP3 and NLRC4 in host defense against Salmonella. J Exp Med. 2010;207:1745–55.
26. Man SM. Inflammasomes in the gastrointestinal tract: infection, cancer and gut microbiota homeostasis. Nat Rev Gastroenterol Hepatol. 2018;15:721–37.
27. Man SM, Hopkins LJ, Nugent E, Cox S, Gluck IM, Tourlomousis P, et al. Inflammasome activation causes dual recruitment of NLRC4 and NLRP3 to the same macromolecular complex. Proc Natl Acad Sci USA. 2014;111:7403–8.
28. Rauch I, Deets KA, Ji DX, von Moltke J, Tenthorey JL, Lee AY, et al. NAIP-NLRC4 inflammasomes coordinate intestinal epithelial cell expulsion with eicosanoid and IL-18 release via activation of caspase-1 and -8. Immunity. 2017;46:649–59.
29. Sellin ME, Muller AA, Felmy B, Dolowschiak T, Diard M, Tardivel A, et al. Epithelium-intrinsic NAIP/NLRC4 inflammasome drives infected enterocyte expulsion to restrict Salmonella replication in the intestinal mucosa. Cell Host Microbe. 2014;16:237–48.
30. Han X, Ding S, Jiang H, Liu G. Roles of macrophages in the development and treatment of gut inflammation. Front Cell Dev Biol. 2021;9:625423.
31. Perkins DJ, Rajaiah R, Tennant SM, Ramachandran G, Higginson EE, Dyson TN, et al. Salmonella typhimurium co-opts the host type I IFN system to restrict macrophage innate immune transcriptional responses selectively. J Immunol. 2015;195:2461–71.
32. Mariathasan S, Weiss DS, Newton K, McBride J, O'Rourke K, Roose-Girma M, et al. Cryopyrin activates the inflammasome in response to toxins and ATP. Nature. 2006;440:228–32.
33. Qi H, Wei J, Gao Y, Yang Y, Li Y, Zhu H, et al. Reg4 and complement factor D prevent the overgrowth of *E. coli* in the mouse gut. Commun Biol. 2020;3:483.
34. Gram AM, Wright JA, Pickering RJ, Lam NL, Booty LM, Webster SJ, et al. Salmonella flagellin activates NAIP/NLRC4 and canonical NLRP3 inflammasomes in human macrophages. J Immunol. 2021;206:631–40.
35. Reyes Ruiz VM, Ramirez J, Naseer N, Palacio NM, Siddarthan IJ, Yan BM, et al. Broad detection of bacterial type III secretion system and flagellin proteins by the human NAIP/NLRC4 inflammasome. Proc Natl Acad Sci USA. 2017;114:13242–7.
36. Smith KD, Andersen-Nissen E, Hayashi F, Strobe K, Bergman MA, Barrett SL, et al. Toll-like receptor 5 recognizes a conserved site on flagellin required for protofilament formation and bacterial motility. Nat Immunol. 2003;4:1247–53.
37. Miao EA, Alpuche-Aranda CM, Dors M, Clark AE, Bader MW, Miller SI, et al. Cytoplasmic flagellin activates caspase-1 and secretion of interleukin 1beta via Ipaf. Nat Immunol. 2006;7:569–75.
38. Ghoneim HE, Thomas PG, McCullers JA. Depletion of alveolar macrophages during influenza infection facilitates bacterial superinfections. J Immunol. 2013;191:1250–9.
39. Wang Y, Wang P, Zhang Y, Xu J, Li Z, Li Z, et al. Decreased expression of the host long-noncoding RNA-GM facilitates viral escape by inhibiting the kinase activity TBK1 via S-glutathionylation. Immunity. 2020;53:1168–81.e7.
40. Lin A, Li C, Xing Z, Hu Q, Liang K, Han L, et al. The LINK-A lncRNA activates normoxic HIF1alpha signalling in triple-negative breast cancer. Nat Cell Biol. 2016;18:213–24.
41. Saha S, Kiran M, Kuscu C, Chatrath A, Wotton D, Mayo MW, et al. Long noncoding RNA DRAIC inhibits prostate cancer progression by interacting with IKK to inhibit NF-kappaB activation. Cancer Res. 2020;80:950–63.
42. Wang C, Li Y, Yan S, Wang H, Shao X, Xiao M, et al. Interactome analysis reveals that lncRNA HULC promotes aerobic glycolysis through LDHA and PKM2. Nat Commun. 2020;11:3162.
43. Koirala P, Huang J, Ho TT, Wu F, Ding X, Mo YY. LncRNA AK023948 is a positive regulator of AKT. Nat Commun. 2017;8:14422.
44. Karki R, Lee E, Place D, Samir P, Mavuluri J, Sharma BR, et al. IRF8 regulates transcription of naips for NLRC4 inflammasome activation. Cell. 2018;173:920–33.e13.
45. Tenthorey JL, Chavez RA, Thompson TW, Deets KA, Vance RE, Rauch I. NLRC4 inflammasome activation is NLRP3- and phosphorylation-independent during infection and does not protect from melanoma. J Exp Med. 2020;217:e20191736.
46. Kofoed EM, Vance RE. Innate immune recognition of bacterial ligands by NAIPs determines inflammasome specificity. Nature. 2011;477:592–5.
47. Qu Y, Misaghi S, Newton K, Maltzman A, Izrael-Tomasevic A, Arnott D, et al. NLRP3 recruitment by NLRC4 during Salmonella infection. J Exp Med. 2016;213:877–85.
48. Hu Z, Zhou Q, Zhang C, Fan S, Cheng W, Zhao Y, et al. Structural and biochemical basis for induced self-propagation of NLRC4. Science. 2015;350:399–404.
49. Zhang L, Chen S, Ruan J, Wu J, Tong AB, Yin Q, et al. Cryo-EM structure of the activated NAIP2-NLRC4 inflammasome reveals nucleated polymerization. Science. 2015;350:404–9.
50. Suzuki S, Franchi L, He Y, Munoz-Planillo R, Mimuro H, Suzuki T, et al. Shigella type III secretion protein MxiI is recognized by Naip2 to induce Nlrc4 inflammasome activation independently of Pkcdelta. PLoS Pathog. 2014;10:e1003926.
51. Wang P, Xue Y, Han Y, Lin L, Wu C, Xu S, et al. The STAT3-binding long noncoding RNA lnc-DC controls human dendritic cell differentiation. Science. 2014;344:310–3.
52. Li Z, Zhang J, Liu X, Li S, Wang Q, Di C, et al. The LINC01138 drives malignancies via activating arginine methyltransferase 5 in hepatocellular carcinoma. Nat Commun. 2018;9:1572.
53. Cao S, Su X, Zeng B, Yan H, Huang Y, Wang E, et al. The gut epithelial receptor LRRC19 promotes the recruitment of immune cells and gut inflammation. Cell Rep. 2016;14:695–707.
54. Su X, Min S, Cao S, Yan H, Zhao Y, Li H, et al. LRRC19 expressed in the kidney induces TRAF2/6-mediated signals to prevent infection by uropathogenic bacteria. Nat Commun. 2014;5:4434.
55. Shang W, Gao Y, Tang Z, Zhang Y, Yang R. The pseudogene Olfr29-ps1 promotes the suppressive function and differentiation of monocytic MDSCs. Cancer Immunol Res. 2019;7:813–27.

ACKNOWLEDGEMENTS

This research was supported by NSFC grants (grant numbers 81901677, 82271779, 91842302, 81970457, and 91629102); The Tianjin Science and Technology Commission (grant number, 18JCZDJC35300); A Ministry of Science and Technology (grant number, 2016YFC1303604); The State Key Laboratory of Medicinal Chemical Biology and the Fundamental Research Funds for the Central University, Nankai university (63191724).

AUTHOR CONTRIBUTIONS

RY designed the research and wrote the paper; YG conducted in vivo and in vitro experiments for identifying mechanisms of action; YY and QZ conducted most of the in vivo experiments and immunoassays; JW, JY, YW, MJ, RW, and XY performed some of the in vitro experiments; JZ, XL offered assistance for the ITC analyses, and YZ offered assistance for the animal experiments. All authors read and approved the final manuscript.

COMPETING INTERESTS

The authors declare no competing interests.

ADDITIONAL INFORMATION

Supplementary information The online version contains supplementary material available at https://doi.org/10.1038/s41423-023-00995-1.

Correspondence and requests for materials should be addressed to Rongcun Yang.